

Article

Fuzzy-Augmented Model Reference Adaptive PID Control Law Design for Robust Voltage Regulation in DC–DC Buck Converters

Omer Saleem ¹, Khalid Rasheed Ahmad ¹ and Jamshed Iqbal ^{2,*}

¹ Department of Electrical Engineering, National University of Computer and Emerging Sciences, Lahore 54770, Pakistan

² School of Computer Science, Faculty of Science and Engineering, University of Hull, Hull HU6 7RX, UK

* Correspondence: j.iqbal@hull.ac.uk

Abstract: This paper presents a novel fuzzy-augmented model reference adaptive voltage regulation strategy for the DC–DC buck converters to enhance their resilience against random input variations and load-step transients. The ubiquitous proportional-integral-derivative (PID) controller is employed as the baseline scheme, whose gains are tuned offline via a pre-calibrated linear-quadratic optimization scheme. However, owing to the inefficacy of the fixed-gain PID controller against parametric disturbances, it is retrofitted with a model reference adaptive controller that uses Lyapunov gain adaptation law for the online modification of PID gains. The adaptive controller is also augmented with an auxiliary fuzzy self-regulation system that acts as a superior regulator to dynamically update the adaptation rates of the Lyapunov gain adaptation law as a nonlinear function of the system's classical error and its normalized acceleration. The proposed fuzzy system utilizes the knowledge of the system's relative rate to execute better self-regulation of the adaptation rates, which in turn, flexibly steers the adaptability and response speed of the controller as the error conditions change. The propositions above are validated by performing tailored hardware experiments on a low-power DC–DC buck converter prototype. The experimental results validate the improved reference tracking and disturbance rejection ability of the proposed control law compared to the fixed PID controller.

Keywords: buck converter; PID controller; model reference adaptive system; Lyapunov gain adjustment law; fuzzy inference; relative rate

MSC: 49N05; 62F35; 93A30; 93C40; 93C42

Citation: Saleem, O.; Ahmad, K.R.; Iqbal, J. Fuzzy-Augmented Model Reference Adaptive PID Control Law Design for Robust Voltage Regulation in DC–DC Buck Converters. *Mathematics* **2024**, *12*, 1893. <https://doi.org/10.3390/math12121893>

Academic Editor: Senthil Krishnamurthy

Received: 29 May 2024

Revised: 13 June 2024

Accepted: 15 June 2024

Published: 18 June 2024



Copyright: © 2024 by the authors. Licensee MDPI, Basel, Switzerland. This article is an open access article distributed under the terms and conditions of the Creative Commons Attribution (CC BY) license (<https://creativecommons.org/licenses/by/4.0/>).

1. Introduction

A buck converter is a DC–DC power converter that steps down the voltage from a higher level to a lower level [1]. It is widely used for efficient power conversion and voltage regulation in electronic systems owing to their compact size, improved conversion efficiency, minimal drop-out voltage, affordable manufacturing expenses, and substantial output power supply [2]. Some of the key applications of the buck converter include power supplies [3], LED lighting systems [4], electronic subsystems in electric vehicles [5], renewable energy conversion systems [6], etc. To eliminate the error between the reference voltage (v_{ref}) and actual output voltage (v_o) of the buck converter, negative feedback control schemes are typically used to continuously change the duty cycle (d) of the circuit's primary switch [7]. The closed-loop control procedures for DC–DC buck converters aim to regulate the output voltage by adjusting the duty cycle of the converter's switch [8]. Nonetheless, the researchers have faced significant difficulty in optimizing the converter's output regulation at the intended reference while considering the input variations and

load fluctuations that affect the system's transient response [9]. The bilinear property of the buck converter poses another challenging control problem. The sudden changes in the circuit configuration within each switching interval are caused by the variations in the state of the switching transistor [10]. Conventional control approaches are ineffective in compensating for the nonlinear discontinuous behavior and the switching losses caused by the high-frequency switching phenomenon in the system [11]. In summary, buck converters play a crucial role in modern power electronic systems, offering efficient voltage conversion. However, addressing control problems is essential to ensure optimal performance and reliability in various applications.

1.1. Literature Review

Several control laws have been proposed in the scientific literature. The proportional–integral–derivative (PID) control scheme, and its variants, are one of the most widely used techniques due to their reliable control yield and simple structure [12]. The proportional term provides an immediate response to the error, the integral term eliminates steady-state errors, and the derivative term anticipates future errors [13]. These actions synergistically aid the controller in rejecting the bounded exogenous disturbances. However, without auxiliary augmentations, their limited degrees of freedom restrict them from addressing un-modeled nonlinearities [14]. The fractional complex order PID controllers tend to show enhanced robustness towards uncertainties than the linear and fractional PID controllers [15]. However, the offline tuning and optimization of a multitude of controller parameters introduced in the control law by the said techniques is a laborious process [16]. The sliding mode controller (SMC) is a nonlinear control technique that ensures robustness against parameter variations and disturbances [17]. It creates a sliding surface in the state space such that the system dynamics are confined to this surface. However, the continuous switching in the control law renders a discontinuous control behavior, which unavoidably increases the ripple content in the state response(s) [18]. The higher-order sliding mode controllers (HOSMCs) tend to effectively reduce chattering in systems as proposed in [19]. However, their reliance upon complex algorithms to compute the higher-order state derivatives adds excessive computation burden and makes them highly sensitive to high-frequency sensor noise [20].

The neural controllers require training data to formulate an accurate inverse control law [21]. Despite its resilience against disturbances, its dependence on large training data sets increases the algorithm's computation burden [22]. The integration of the CNN approximation tool with the conventional backstepping scheme yields a robust regulatory control of output voltage in DC–DC converters [23]. However, its computational realization is quite complex and can be problematic in systems with limited computational abilities. The fuzzy logic control schemes are particularly useful when the system's nonlinear dynamics are difficult to model accurately or when precise mathematical control laws are impractical [24]. In DC–DC converters, the fuzzy logic controller tends to adjust the duty cycle based on fuzzy rules that map input variables (such as output voltage error and change in error) to output control actions [25].

The linear quadratic regulator (LQR) provides optimal control in terms of minimizing a quadratic cost function, which can result in superior performance compared to other control techniques [26]. However, it relies on an accurate system model and deviations from the model under disturbances lead to suboptimal performance or instability [27]. The model predictive control (MPC) scheme uses the system's dynamic model to predict future behavior and optimize control actions over a finite time horizon [28]. However, despite its robustness, solving an optimization problem at each control step can be computationally intensive [29]. The nonlinear H-infinity controllers are renowned for their robust control yield [30]. However, their formulation requires an accurate mathematical model of the system, and they impose mathematical complexity in design and implementation [31]. The backstepping controllers are used to deal with nonlinearities occurring in multi-variable systems [32]. However, to ensure stability, backstepping designs can

sometimes be overly conservative, leading to suboptimal performance in terms of response time and control effort [33].

The adaptive controllers dynamically adjust the critical controller parameters to optimize the controller's flexibility and adaptability to disturbances and parametric uncertainties [34]. The model reference adaptive controllers (MRACs) are designed to adapt to uncertainties and variations in the system, making them suitable for systems with unknown or time-varying dynamics [35]. They adaptively re-adjust the controller gains to maintain robust performance even when the system parameters change or deviate from the nominal values. The gain adjustment law is derived using the Lyapunov stability theorem [36]. Despite their inherent flexibility, the designing and tuning of critical parameters in the MRAC law can be complex, especially for systems with high-order dynamics or complex nonlinearities [37]. An ill-postulated MRAC law results in slow convergence of the adaptive gains, affecting the overall control performance [38]. The fuzzy-augmented MRAC procedures are formulated by employing a fuzzy adaptive system, which acts as a superior regulator to dynamically reconfigure the critical controller parameters of the traditional MRAC law [39]. This augmentation improves the controller's flexibility, which enhances the adaptability and robustness of MRAC by leveraging the fuzzy self-regulator's capability to handle controller design imprecisions as well as the intrinsic nonlinearities and parametric variations in the system [40]. This scheme is especially suitable for application in dynamic and uncertain environments where precise mathematical modeling is challenging.

1.2. Main Contribution

The main contribution of this article is the formulation of an online model reference adaptive optimal PID control procedure that robustifies the performance of buck converters against load transients and input fluctuations. The ubiquitous LQR-based PID controller is employed as the baseline control technique owing to its optimal and asymptotically stable control yield. To enhance the robustness and flexibility of the control scheme against exogenous disturbances, a pre-calibrated state space MRAC is designed that tracks the output of the aforementioned LQ-PID controller output as its reference. To further optimize the MRAC-driven PID controller's error convergence rate and damping control strength against disturbances, it is retrofitted with an auxiliary fuzzy self-regulation system that acts as a superior regulator to dynamically adjust the adaptation rates linked with the MRAC's Lyapunov gain adjustment law. The online updates in the adaptation rates are dictated by the real-time variations in the system's relative rate. The three salient contributions of the paper are thus listed below:

1. Formulation of a well-postulated MRAC-based PID control law for the buck converter that tracks the output of the baseline LQ-PID control law.
2. Robustification of the designed MRAC-based PID control law by augmenting it with a pre-configured fuzzy self-regulating system that uses the system's output voltage error and its relative rate to dynamically adjust the MRAC's inner adaptation rates.
3. Experimental validation of the proposed fuzzy-augmented MRAC-based PID control law by performing tailored hardware experiments on a low-power DC–DC buck converter prototype.

1.3. Innovative Features of the Proposed Control Law

The proposed control scheme undertakes to address several challenges faced by conventional control schemes. Firstly, the proposed MRAC tracks the output of an optimal and inherently stable LQ-PID controller as its reference to adaptively modulate the gains. This provision aids the controller in preserving the system's asymptotic stability while mimicking the optimum behavior to maintain a reasonable control input economy and avoid chattering in the state response(s). However, unlike the LQ-PID controller, the online gain adjustment makes the MRAC more robust to model inaccuracies. Unlike the

fractional order controllers, the proposed scheme does not depend on a multitude of parameters that have to be tuned offline. Secondly, the fixed adaptation rates of the MRAC law limit its operability, rendering it ineffective against abrupt state error variations. The aforesaid problem is addressed by augmenting the MRAC with a model-free fuzzy inference system that is driven by the system's relative rate. The fuzzy self-regulation of the adaptation rates obviates the necessity to predefine and affix the adaptation rates, thus increasing the controller's design flexibility. Instead of depending on mere magnitudes of the state error variables, the fuzzy self-regulation system relies upon the relative rate feedback. This augmentation adaptively modulates the said adaptation rates in response to the variations in the fastness (or sluggishness) of the state response as it moves away or towards the reference voltage signal. The fuzzy nonlinear scaling of the adaptation rates further increases the controller's agility, allowing it to flexibly adapt the applied control tightness as per the requirements. The fuzzy function can be computed to update the gains in a single step after the sampling interval. Thus, unlike neural adaptive systems, fuzzy nonlinear scaling does not put any recursive computational burden on the embedded processor.

As a result of all these features, the system exhibits a faster response speed with strong damping against disturbances. Furthermore, this configuration also avoids compromise between the system's steady-state and transient performance. The comparative analysis of the proposed control law with existing state-of-the-art controllers based on different parameters is summarized in Table 1.

Table 1. Comparative analysis of the proposed work with existing state-of-the-art.

Performance Parameter	COPID [15]	HOSMC [20]	CNN [23]	LQ-PID [26]	H-inf [30]	Backstep [32]	MRAC [35]	Proposed Scheme
Error minimization	Good	Better	Good	Bad	Good	Fair	Good	Good
Asymptotic stability	Yes	Yes	Yes	Yes	Yes	Difficult	Yes	Yes
Control economy	Fair	Bad	Bad	Better	Fair	Bad	Fair	Better
Disturbance rejection	Good	Best	Better	Bad	Good	Fair	Good	Better
Chattering suppression	Good	Fair	Fair	Good	Good	Good	Better	Better
Mathematical complexity	Medium	High	High	Low	High	High	Low	Low
Computation burden	Medium	High	High	Low	High	High	Low	Medium
Parameter tuning needed	High	Medium	High	Low	Low	High	Low	Medium

The idea of enhancing the MRAC-driven PID controller's flexibility and robustness against the exogenous disturbances occurring in DC–DC buck conversion applications, by using the system's relative rate information to online adjust its inner adaptation rates, has never been proposed in the scientific literature thus far. Hence, this paper mainly focuses on the execution of this novel idea.

The remaining paper is organized as follows. The system's state space model and the baseline LQ-PID compensator design are discussed in Section 2. The formulation of the basic MRAC-based PID control law and the design of the fuzzy inference system for the systematic constitution of the proposed fuzzy-augmented MRAC-based PID controller are respectively presented in Sections 3 and 4. The experimental analysis and validation of the proposed control procedure are presented in Section 5. Finally, the article is concluded in Section 6.

2. System Description

The DC–DC buck converter serves to step down the higher DC voltage input to a lower voltage level at the output. Figure 1 displays the schematic of the synchronous buck converter circuit [41]. The rapid switching of the primary transistor Q_1 serves to control the flow of current through the circuit. To deliver and regulate the desired value of average voltage at the output, the duty-cycle ratio, d , of the switching period of Q_1 's gating signal is suitably adjusted [41]. The relationship between the input voltage v_{in} and the output voltage v_o is expressed in (1).

$$v_o = dv_{in} \tag{1}$$

such that, $d = \frac{t_{on}}{t_{on} + t_{off}}$, where t_{on} is the on-time and t_{off} is the off-time of the switching period. The transistor Q_1 is connected to an inductor, L . When Q_1 is turned on, current flows through the inductor and stores energy in its magnetic field. The output capacitor, C , helps to smooth out the ripples in v_o . When Q_1 is turned off, the magnetic field collapses and causes the inductor to release stored energy. This energy is transferred to the output capacitor and load. The secondary transistor Q_2 is placed in parallel with the load and turned on to provide a path for the inductor current when the switching element is turned off. To complete the circuit loop during t_{on} and t_{off} , transistor Q_1 is operated during t_{on} while Q_2 is operated during t_{off} . In this research, a state feedback voltage control law is formulated that operates on the state error variables; namely, the error in v_o with respect to a reference v_{ref} , error integral, and error derivative to optimally control the aforementioned switching transistors, which aids in regulating the converter's output under disturbances. The system's closed-loop control block diagram is shown in Figure 2.

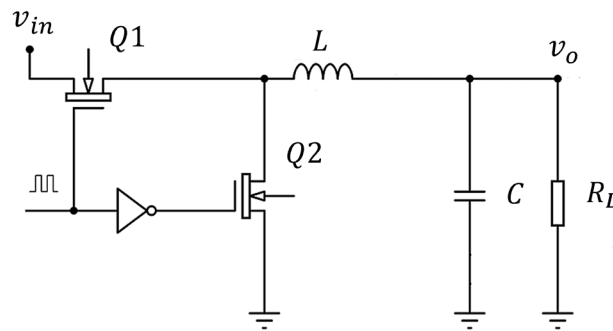


Figure 1. Simplified schematic of the buck converter [41].

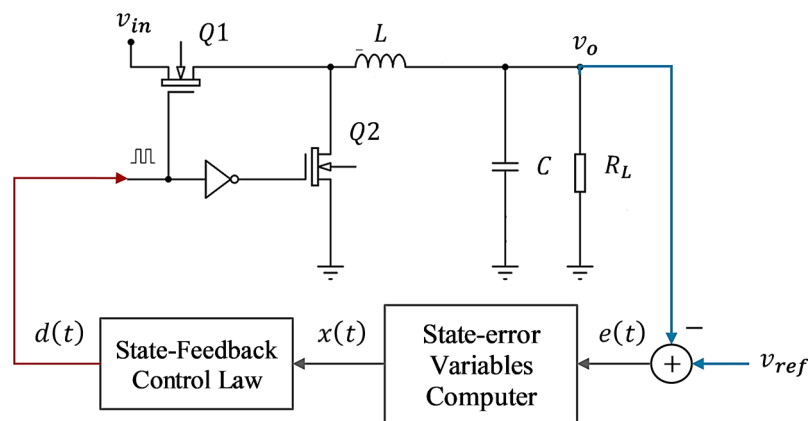


Figure 2. Closed-loop control block diagram of the system.

2.1. State Space Model

The second-order small signal model of the DC–DC buck converter has already been derived in previous works [26,41]. The second-order transfer function representing the dynamics between the input duty cycle to output voltage, in the frequency domain, is given in (2), [26].

$$\frac{v_o(s)}{d(s)} = \left(\frac{v_{in}}{LC}\right) \left(\frac{sCr_c + 1}{s^2 + \left(\frac{1}{R_L C} + \frac{r_c + r_L}{L}\right)s + \frac{1}{LC}} \right) \tag{2}$$

where s is the Laplace operator, and $v_o(s)$ and $d(s)$ represents the output voltage signal and duty cycle signal in the frequency domain, respectively. The converter model also includes the parasitic impedances r_c and r_L , which represent the circuit's equivalent-series-resistance (ESR) and equivalent-series-inductance (ESL), respectively. The model parameters of the buck converter c , used in this research, are identified in Table 2. As shown in Table 2, the magnitudes of the parameters C and r_c are quite small. Hence, the contribution of these parameters in the numerator of the expression is ignored. The simplified transfer function is expressed in (3).

$$\frac{v_o(s)}{d(s)} = \frac{\frac{v_{in}}{LC}}{s^2 + \left(\frac{1}{R_L C} + \frac{r_c + r_L}{L}\right)s + \frac{1}{LC}} \tag{3}$$

The tracking error between the reference voltage and the output voltage of the buck regulator is expressed as follows.

$$e(t) = v_{ref} - v_o(t) \tag{4}$$

where v_{ref} is the reference voltage. It is to be noted that the reference (setpoint) signal does not influence control law design in typical regulatory control problems. Therefore, the expression becomes $v_o(t) = -e(t)$ when the value of v_{ref} is ignored. The system's transfer function is thus modified by the aforementioned substitution.

$$\frac{-e(s)}{d(s)} = \frac{\frac{v_{in}}{LC}}{s^2 + \left(\frac{1}{R_L C} + \frac{r_c + r_L}{L}\right)s + \frac{1}{LC}} \tag{5}$$

Table 2. Model parameters of the buck converter prototype [41].

Parameters	Description	Value	Units
R_L	Load resistor	10	Ω
L	Inductor	220	mH
C	Capacitor	2700	μF
r_c	Capacitor's ESR	0.04	Ω
r_L	Capacitor's ESL	0.06	Ω
v_{in}	Input voltage	24.0	V
v_{ref}	Output voltage	10.0	V

The said transfer function can be rewritten as shown in (6).

$$\left(s^2 + \left(\frac{1}{R_L C} + \frac{r_c + r_L}{L}\right)s + \frac{1}{LC}\right)e(s) = -\left(\frac{v_{in}}{LC}\right)d(s) \tag{6}$$

This equation's inverse Laplace transform yields the following second-order differential Equation (7). The system is considered to have zero initial conditions.

$$\ddot{e}(t) + \left(\frac{1}{R_L C} + \frac{r_c + r_L}{L}\right)\dot{e}(t) + \left(\frac{1}{LC}\right)e(t) = -\left(\frac{v_{in}}{LC}\right)d(t) \tag{7}$$

To derive the state equations, the following state variables are selected [41].

$$x_1(t) = \int e(t) dt, \quad x_2(t) = e(t), \quad x_3(t) = \dot{e}(t) \tag{8}$$

Finally, the aforementioned differential equation is used to derive the following set of state equations.

$$\begin{aligned} \dot{x}_1(t) &= x_2(t), \\ \dot{x}_2(t) &= x_3(t), \\ \dot{x}_3(t) &= -\left(\frac{1}{LC}\right)x_2(t) - \left(\frac{1}{R_L C} + \frac{r_c + r_L}{L}\right)x_3(t) - \left(\frac{v_{in}}{LC}\right)d(t). \end{aligned} \tag{9}$$

For a linear dynamical system, the state space representation is expressed in (10).

$$\dot{x}(t) = \mathbf{A}x(t) + \mathbf{B}u(t), \quad y(t) = \mathbf{C}x(t) + \mathbf{D}u(t) \tag{10}$$

where $x(t)$ is the state vector, $y(t)$ is the output vector, $u(t)$ is the control input signal, \mathbf{A} is the system matrix, \mathbf{B} is the input matrix, \mathbf{C} is the output matrix, and \mathbf{D} is the feed-forward matrix. The system’s state and input vector are provided in (11).

$$x(t) = \left[\int e(t) dt \quad e(t) \quad \dot{e}(t) \right]^T, \quad u(t) = d(t) \tag{11}$$

The nominal linear state space model of the buck converter is given by (12).

$$\mathbf{A} = \begin{bmatrix} 0 & 1 & 0 \\ 0 & 0 & 1 \\ 0 & a_1 & a_2 \end{bmatrix}, \quad \mathbf{B} = \begin{bmatrix} 0 \\ 0 \\ b \end{bmatrix}, \quad \mathbf{C} = \begin{bmatrix} 1 & 0 & 0 \\ 0 & 1 & 0 \\ 0 & 0 & 1 \end{bmatrix}, \quad \mathbf{D} = \begin{bmatrix} 0 \\ 0 \\ 0 \end{bmatrix} \tag{12}$$

where

$$a_1 = -\left(\frac{1}{LC}\right), \quad a_2 = -\left(\frac{1}{R_L C} + \frac{r_c + r_L}{L}\right), \quad b = -\left(\frac{v_{in}}{LC}\right).$$

2.2. Baseline LQ-PID Compensator Design

In this section, an LQR-driven PID controller is developed for the DC–DC buck converter system [41,42]. The LQR is a popular optimal control technique used for regulating the linear systems described by state space equations [1]. It is a state feedback control law, which means that the control input is determined as a linear function of the state variables. The optimal control law is designed to minimize the quadratic cost function (QCF) over an infinite time horizon while ensuring stability and satisfying any constraints on the system [43]. The QCF, expressed in (13), is typically defined as the sum of the quadratic variations in the system’s states and the control effort.

$$J_{lq} = \frac{1}{2} \int_0^\infty (x(t)^T \mathbf{Q}x(t) + u(t)^T \mathbf{R}u(t)) dt \tag{13}$$

where $\mathbf{Q} \in \mathbb{R}^{4 \times 4} \geq 0$ is a pre-calibrated state penalty matrix while $\mathbf{R} \in \mathbb{R} > 0$ is a pre-calibrated control penalty matrix. Each element of the \mathbf{Q} and \mathbf{R} matrices represent the weight or cost associated with the corresponding state variable or control input, respectively. A higher value of an element implies that minimizing the deviation of that state variable or input carries more importance in the control objective [26]. The penalty matrices constituted for the buck converter system used in this research are defined as

$$\mathbf{Q} = \text{diag}(q_I \quad q_P \quad q_D), \quad \mathbf{R} = \rho \tag{14}$$

where $q_x \geq 0$ and $\rho > 0$ are the elements of the \mathbf{Q} and \mathbf{R} matrices, respectively. The tuning procedure covered in Section 2.3 is used to precisely calibrate the elements of each matrix offline. The solution to the LQR problem involves solving an algebraic Riccati equation (ARE) using the pre-calibrated set of \mathbf{Q} and \mathbf{R} matrices, which provides a symmetric positive definite matrix \mathbf{P} . The ARE is expressed in (15), [43].

$$\mathbf{A}^T \mathbf{P} + \mathbf{P} \mathbf{A} - \mathbf{P} \mathbf{B} \mathbf{R}^{-1} \mathbf{B}^T \mathbf{P} + \mathbf{Q} = 0 \tag{15}$$

where $\mathbf{P} \in \mathbb{R}^{4 \times 4}$. This solution yields the following state feedback gain vector \mathbf{K} .

$$\mathbf{K} = \mathbf{R}^{-1} \mathbf{B}^T \mathbf{P} \tag{16}$$

where $\mathbf{K} = [K_I \quad K_P \quad K_D]$. The optimal linear control law is expressed as follows:

$$u(t) = -Kx(t) \tag{17}$$

The expansion of the said control law yields the following LQ-PID controller.

$$u(t) = -K_p e(t) - K_I \int e(t) dt - K_D \dot{e}(t) \tag{18}$$

The block diagram of the LQ-PID control law is shown in Figure 3. The asymptotic stability of the derived LQ-PID control law is demonstrated via the following Lyapunov function [43].

$$V(t) = x(t)^T P(t)x(t) > 0, \text{ for } x(t) \neq 0 \tag{19}$$

The Lyapunov function’s first derivative is represented as shown below.

$$\begin{aligned} \dot{V}(t) &= 2x(t)^T P \dot{x}(t) \\ &= 2x(t)^T P(A - BK(t))x(t) \\ &= 2x(t)^T P(A - BR^{-1}B^T P)x(t) \\ &= x(t)^T (PA + A^T P)x(t) - 2x(t)^T (PBR^{-1}B^T P)x(t) \end{aligned} \tag{20}$$

By substituting the Equation (14), the derivative $\dot{V}(t)$ simplifies as given in (21).

$$\dot{V}(t) = -x(t)^T Qx(t) - x(t)^T (PBR^{-1}B^T P)x(t) < 0 \tag{21}$$

If $Q = Q^T \geq 0$ and $R = R^T > 0$, then $\dot{V}(t)$ is always negative semi-definite. This criterion is sufficient to ensure the proposed controller’s closed-loop stability. The switching transistor control input, $u(t)$, is saturated between 0 and 1 via the following formulation.

$$\text{sat}(u(t)) = \begin{cases} 1, & u(t) \geq 1 \\ u(t), & 0 < u(t) < 1 \\ 0, & u(t) \leq 0 \end{cases} \tag{22}$$

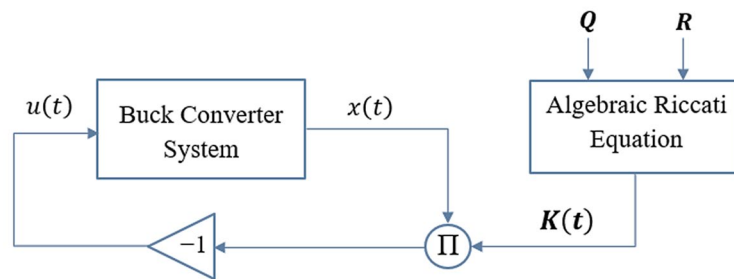


Figure 3. Block diagram of the LQ-PID control law.

2.3. Parameter Tuning Procedure

According to J_{lq} , the LQ-PID regulator’s formulation is dependent on the changes in the system’s control input and states. However, to guarantee an optimum control yield, it is crucial to provide the aforementioned variables with the proper weights. Due to poor engineering intuition or the designer’s experience limitations, the trial-and-error-based configurations of Q and R matrices might not always yield precise position regulation and transient recovery behavior [26]. Therefore, a new objective function is presented in this section that considers the settling time t_s , magnitude of the peak overshoot M_p , tracking error variations, and the input variations in the system’s time domain response.

$$J_a = t_s^2 + |OS|^2 + \int_0^\infty (|e(t)|^2 + |u(t)|^2) dt \tag{23}$$

This objective function is minimized to acquire the best-fit solutions of the Q and R matrices.

To impose an equal impact on all the minimization criteria, equal weights are set for each component of the cost function represented above. The search range for all the

elements of the \mathbf{Q} and \mathbf{R} matrices is $[0, 10]$. Equal (unity) weight is applied to each state variable to start the offline tuning procedure. Hence, the initial matrix is set at $\mathbf{Q} = \text{diag}(1 \ 1 \ 1)$ and $\mathbf{R} = 1$. The exploration for the best-fit parameters is then coordinated by the tuning algorithm in the direction of the steepest gradient descent of the cost function J_d . Figure 4 demonstrates the process used to tune the parameters [44]. The method for carrying out the trial experiments for parameter adjustment is detailed in Section 5.1.

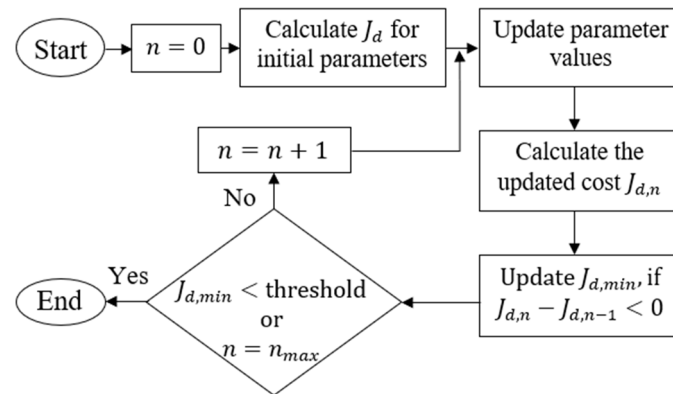


Figure 4. Flow chart of the parameter tuning process.

In every tuning iteration, the LQ-PID controller gains are empirically tweaked and the controller is assigned to regulate the converter's v_o at 10.0 V for 5.0 sec to solve the cost function J_d and evaluate the cost of the current iteration $J_{d,n}$; where n is the iteration number. The process of minimizing the objective cost function is discussed as follows: If the cost of the current iteration $J_{d,n}$ is found to be lower than the cost of the previous iteration $J_{d,n-1}$, then the local minimum cost variable J_{min} is altered. This arrangement ensures that the search is proceeding along the declining gradient of J_d . When the algorithm achieves the maximum number of iterations (n_{max}) allowed or $J_{d,min} < \delta$, where δ is a predefined cost threshold, the search for the optimal parameter values is terminated [44]. The said threshold is determined heuristically via preliminary runs of the algorithm. By conducting pilot runs with various thresholds and evaluating the resulting parameters, the aforementioned thresholds are selected to balance the algorithm's computational burden and solution quality while avoiding its premature termination. In this research, the $J_{d,min}$ for initial settings of \mathbf{Q} and \mathbf{R} is recorded as $J_{d,min}^0 \approx 1.28 \times 10^6$. A scaled-down value of $J_{d,min}^0$ is then used as the termination condition. A scale of 0.008 is thus selected to avoid unnecessary computational burden and ensure faster convergence of the algorithm. A larger scale value places an excessive iterative computational burden while a smaller one leads to premature termination. Thus, the algorithm is terminated when $J_{d,min}$ approaches $0.008 J_{d,min}^0$. Correspondingly, the values of the threshold for $J_{d,min}$ and n_{max} are preset at 1×10^4 and 40, respectively, in this study.

The optimal set of state costs and control costs are $\mathbf{Q} = \text{diag}(9.64 \ 1.55 \ 0.21)$ and $\mathbf{R} = 1.05$, respectively. The corresponding state feedback gain vector is $\mathbf{K} = [-3.17 \ -1.82 \ -0.24]$.

3. Basic MRAC-Based PID Control Law

The traditional MRAC law minimizes the tracking error between the outputs of the LQ-PID-regulated reference model and the real system by updating the controller gain vector \mathbf{K} online using a Lyapunov function [45]. The linear system presented in (10) is considered to formulate the traditional MRAC law.

The objective is to build an adaptive control rule that mimics the response exhibited by LQ-PID-regulated reference model (\mathbf{A}_{ref}), as represented by the following autonomous system [46].

$$\dot{x}_{ref}(t) = A_{ref}x_{ref}(t) \tag{24}$$

The formulation of MRAC law necessitates an asymptotically stable reference model. Thus, the LQ-PID-regulated closed-loop buck converter system is employed as a reference model. The adaptive controller thus designed optimality tracks and attains using the baseline established by A_{ref} , which is identified by the LQ-PID controller constituted previously. The proposed adaptive control law is given in (25).

$$u(t) = -K(t)x(t) \tag{25}$$

where $K(t) = [K_I(t) \ K_p(t) \ K_D(t)]$ represents the time-varying state feedback gain vector whose elements are adaptively modified online via the MRAC scheme [40]. The actual system's closed-loop description is provided in (26).

$$\dot{x}(t) = (A - BK_S)x(t) = A_S(K_S)x(t) \tag{26}$$

where the system matrix A_S is driven by the vector K_S .

Compatibility condition: In general, it is quite hard to obtain a gain vector K_S such that the actual system's model becomes identical to that of the reference model. However, there exists another vector \hat{K}_S that can be stated as follows to provide a sufficient condition for tracking the reference model [47]:

$$A_c(\hat{K}_a) = A_{ref} = A - B\hat{K}_S \tag{27}$$

This criterion indicates that the columns of $A - A_{ref}$ are linear combinations of matrix B columns. In this study, the gain vector $\hat{K}_S = K$ is used to identify the A_{ref} . The difference between the state vectors of the real system and the reference system is calculated by the tracking error vector, $\varepsilon(t)$, expressed in (28).

$$\varepsilon(t) = x(t) - x_{ref}(t) \tag{28}$$

The convergence rate of the online adaptation mechanism is directed by the said tracking error vector. The tracking error's derivative is expressed as shown in (29).

$$\dot{\varepsilon}(t) = \dot{x}(t) - \dot{x}_{ref}(t) \tag{29}$$

This derivative can also be written by substituting the Equations (10) and (24).

$$\dot{\varepsilon}(t) = Ax(t) + Bu(t) - A_{ref}x_{ref}(t) \tag{30}$$

The tracking error derivative's formulation is as modified by concurrently adding and eliminating the term $A_{ref}x(t)$, on the right-hand side of (30), as shown below.

$$\begin{aligned} \dot{\varepsilon}(t) &= Ax(t) + Bu(t) - A_{ref}x_{ref}(t) + A_{ref}x(t) - A_{ref}x(t) \\ &= A_{ref}x(t) - A_{ref}x_{ref}(t) + Bu(t) + Ax(t) - A_{ref}x(t) \\ &= A_{ref}(x(t) - x_{ref}(t)) + Bu(t) + (A - A_{ref})x(t) \end{aligned} \tag{31}$$

Using the substitutions, $A - A_{ref} = B\hat{K}_S$ from (15), $u(t) = -K(t)x(t)$ from (13), the tracking error derivative's expression is rewritten as shown in (32).

$$\begin{aligned} \dot{\varepsilon}(t) &= A_{ref}\varepsilon(t) - BK(t)x(t) + B\hat{K}_Sx(t) \\ &= A_{ref}\varepsilon(t) - B(K(t) - \hat{K}_S)x(t) \end{aligned} \tag{32}$$

Using the property of matrix algebra, $XY = Y^T X^T$; where X and Y are arbitrary matrices, the expression of $\dot{\varepsilon}(t)$ is modified as shown in (33).

$$\dot{\varepsilon}(t) = A_{ref}\varepsilon(t) - Bx(t)^T (K(t)^T - \hat{K}_S^T) \tag{33}$$

Using the substitution $\delta = -Bx(t)^T$, the tracking error derivative is finally expressed as shown in (34).

$$\dot{\varepsilon}(t) = A_{ref}\varepsilon(t) + \delta (K(t)^T - \hat{K}_S^T) \tag{34}$$

While simplifying the tracking error derivative's formula, it is assumed that all requirements for accurate model tracking have been satisfied. The online model reference

gain adjustment law that dynamically updates the state feedback gains $\mathbf{K}(t)$ is constructed using the following Lyapunov function [40].

$$W(\varepsilon, K_a) = \frac{1}{2} \left[\alpha_o \varepsilon(t)^T \bar{\mathbf{P}} \varepsilon(t) + \left(\mathbf{K}(t)^T - \hat{\mathbf{K}}_s^T \right)^T \left(\mathbf{K}(t)^T - \hat{\mathbf{K}}_s^T \right) \right] \quad (35)$$

where α_o is the preconfigured positive semi-definite diagonal matrix representing the adaptation rates associated with each state feedback gain, and $\bar{\mathbf{P}}$ is a positive definite symmetric matrix that is evaluated by solving the following equation.

$$\mathbf{A}_{ref}^T \bar{\mathbf{P}} + \bar{\mathbf{P}} \mathbf{A}_{ref} = -\mathbf{Q} \quad (36)$$

The matrix α is represented as shown below.

$$\alpha_o = \text{diag}(\alpha_{I,o} \quad \alpha_{P,o} \quad \alpha_{D,o}) \quad (37)$$

The adaptation rates $\alpha_{I,o}$, $\alpha_{P,o}$, and $\alpha_{D,o}$ are heuristically optimized by using the parameter tuning methodology discussed in Section 2.3. The search space of these adaptation rates is bounded between [0, 10]. The initial matrix is set at $\alpha_o = \text{diag}(1 \quad 1 \quad 1)$. The values of adaptation rates thus optimized and used in this work are given by, $\alpha_o = \text{diag}(2.78 \quad 1.15 \quad 0.18)$. It is to be noted that if \mathbf{A}_{ref} is stable, then there would always be two positive definite matrices, $\bar{\mathbf{P}}$ and \mathbf{Q} . The expression for the derivative of $W(\cdot)$ is presented as follows [40]:

$$\dot{W}(\varepsilon, K_a) = -\frac{1}{2} \alpha_o \varepsilon(t)^T \mathbf{Q} \varepsilon(t) + \left(\mathbf{K}(t)^T - \hat{\mathbf{K}}_s^T \right)^T \left(\dot{\mathbf{K}}(t)^T + \alpha_o \delta^T \bar{\mathbf{P}} \varepsilon(t) \right) \quad (38)$$

The Lyapunov function's derivative $\dot{W}(\varepsilon, K_a)$ is always negative definite if,

$$\dot{\mathbf{K}}(t)^T = -\alpha_o \delta^T \bar{\mathbf{P}} \varepsilon(t) \quad (39)$$

This condition satisfies the convergence of $\varepsilon(t)$ to zero, and thus, acts as the stable adaptive gain adjustment mechanism for the control law. After appropriate substitutions, the derived online gain adjustment law is rewritten as shown below.

$$\dot{\mathbf{K}}(t) = \left(\alpha_o x(t) \mathbf{B}^T \bar{\mathbf{P}} \varepsilon(t) \right)^T \quad (40)$$

The gain adaptation law is implemented in the control software by programming the following solution of the first-order differential equation, expressed below. The control software calculates the updated controller gains, after every sampling interval, by computing the solution of the following first-order differential equation.

$$\mathbf{K}(t) = \mathbf{K}(0) + \int_0^t \left(\alpha_o x(t) \mathbf{B}^T \bar{\mathbf{P}} \varepsilon(t) \right)^T dt \quad (41)$$

The state feedback gain vector $\mathbf{K} = [-3.17 \quad -1.82 \quad -0.24]$, prescribed in Section 2.3, serves as $\mathbf{K}(0)$ in (28). The time-varying gain vector $\mathbf{K}(t)$ thus acquired is used to realize the baseline MRAC law, $u(t) = -\mathbf{K}(t)x(t)$. This MRAC law is expanded, and the corresponding adaptive PID controller formulation is expressed as shown in (42).

$$u(t) = -K_p(t)e(t) - K_I(t) \int e(t) dt - K_D(t)\dot{e}(t) \quad (42)$$

The block diagram of the traditional MRAC-based PID (MRA-PID) control law is shown in Figure 5.

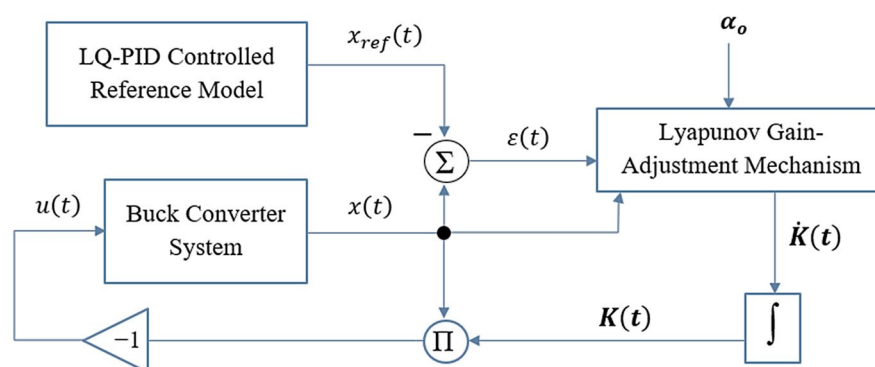


Figure 5. Block diagram of the MRA-PID control law.

4. Proposed Control Methodology

The Lyapunov gain adjustment law’s sensitivity and convergence rate are directly impacted by the adaptation rate matrix α [38]. The selection of a trivial set of fixed adaptation rates typically establishes a compromise between the system’s tracking performance, robustness against disturbances, transient speed, and energy efficiency [40]. A higher adaptation rate allows the controller to respond more quickly to changes in the system, leading to faster transient response, better tracking of desired references, and improved overall performance. However, it also requires more computational resources and energy for parameter updates. On the contrary, a lower adaptation rate slows the response speed and prevents the controller from keeping up with rapid changes in the system, leading to poor tracking performance. However, it also consumes less control energy and potentially yields better noise rejection.

To synergistically combine the benefits of the higher and lower values of the adaptation rates in the MRA-PID design, the adaptation rates are dynamically adjusted online as the state error conditions change by using a pre-calibrated fuzzy self-regulation (FSR) system. The FSR system ensures smooth and bounded commutation of the adaptation rates as the system’s operating conditions vary. The proposed methodology obviates the necessity to preset the adaptation rates offline that only yield a sub-optimal performance. This also makes the design process relatively less labor-intensive. The augmentation of the MRA-PID controller with a pre-calibrated FSR system is simple yet effective in compensating for uncertainties and random disturbances. The proposed procedure upholds the original structure of the MRA-PID controller while retrofitting the critical controller parameters with auxiliary tools to address the nonlinear disturbances. This arrangement increases the controller’s degrees of freedom, thus harnessing its ability to handle a wider range of operating conditions as compared to its traditional counterpart. This makes it more adaptable and flexible to efficiently manipulate the damping control activity as the error conditions vary. The proposed augmentation does not necessitate the requirement of a separate set of stability proofs or conditions. The traditional MRA-PID controller is still operating at the core while FSR assists in robustifying its behavior under perturbations; therefore, it is sufficient to uphold the originally prescribed stability conditions.

The fuzzy adaptive system is employed in this research primarily because it can be easily integrated with traditional control methods to create a hybrid control system that leverages the strengths of multiple approaches. Augmentation of a customized fuzzy system with linear controllers helps them manage and adapt to the nonlinear behavior of complex systems. The fuzzy augmented systems are robust in environments where exact mathematical models are difficult to obtain or where system parameters are subject to variation. Unlike neural adaptive systems, fuzzy systems are not computationally intensive as they do not require large training data sets to yield robust control effort. Instead, they can be easily implemented in real time using the available open software and toolboxes. Unlike traditional adaptation schemes that require precise mathematical

models or closed-form solutions, fuzzy adaptive systems can be designed with minimal mathematical modeling. This simplifies the development process, especially for complex systems where accurate models are hard to derive. Furthermore, the fuzzy systems use linguistic variables, which allow for the incorporation of expert knowledge and human reasoning into the control strategy. This makes the design of the adaptation scheme more intuitive and flexible, as it can mimic human decision-making processes. This design flexibility also helps in empirically configuring the shape and form of the consequent nonlinear scaling function, which yields smooth transitions between control actions, reducing the risk of abrupt changes that could destabilize the system. This behavior is typically hard to track with hyperbolic or sigmoidal functions [38].

The fuzzy rules are constituted based on the normalized absolute value of the voltage error, $e_v(t)$, and the normalized relative rate of the response, $r_v(t)$. By incorporating relative rate feedback, the controller can react quickly and accurately to changes in the system's response speed. This leads to improved transient response and helps the system reach its desired state more efficiently. Moreover, the relative rate helps the controller anticipate the system's dynamic speed (fastness or sluggishness) as well as future error trends, allowing it to make more informed adjustments. This predictive capability can reduce the magnitude of overshoot (or undershoot), leading to a more robust system with fewer oscillations. The detailed design of the proposed control scheme is methodically discussed in the following sub-sections.

4.1. Relative Rate Calculation

The relative rate feedback directs the fuzzy self-regulation mechanism regarding the dynamic speed (fastness or sluggishness) of the system's response as it deviates from the reference signal during initial start-up and transient disturbances, or vice versa [48].

As illustrated in Figure 6, the system's relative rate typically varies from fast to moderate to slow as the response drifts away from the reference signal and transits from equilibrium (or steady state) to transient state [49]. Self-regulating the adaptation rates of the MRAC law as per the changes in the system's relative rate tends to further improve the controller's agility and responsiveness, which in turn aids in efficiently reconfiguring the control trajectory under exogenous disturbances. The correlation of the system's error velocity and error acceleration with the system's response is described in Table 3 [48].

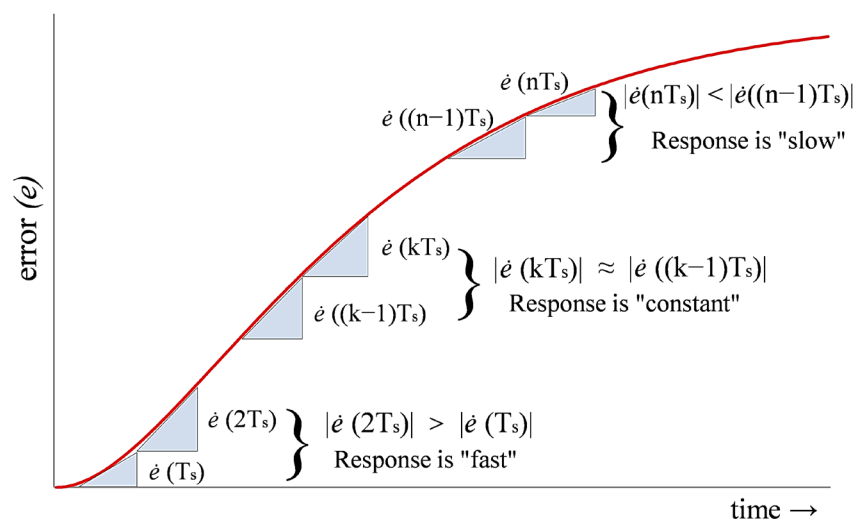


Figure 6. Changes in the system's relative rate [48].

Table 3. Correlation between error velocity, error acceleration, and response.

$\dot{e}(t)$	$\ddot{e}(t)$	System's Response
Positive	Positive	Fast
Positive	Zero	Moderate
Positive	Negative	Slow
Negative	Positive	Slow
Negative	Zero	Moderate
Negative	Negative	Fast

It is evident from Table 3 that the system's response is characterized as slow when the error velocity and acceleration have opposite polarities. Conversely, the system is characterized as fast when the two error variables have the same polarity.

The response is characterized as moderate when the error velocity is constant. Hence, the system's relative rate at a given time can be computed simply by multiplying the system's instantaneous error velocity $\dot{e}(t)$ with its instantaneous error acceleration $\ddot{e}(t)$ [49]. This product is then fed to a bounded and odd symmetric nonlinear function to uphold the aforementioned rationale while normalizing the output between 0 and +1. The system's normalized relative rate, $r_v(t)$, is thus computed as follows:

$$r_v(t) = 0.5 + 0.5 \tanh(\dot{e}(t) \times \ddot{e}(t)) \tag{43}$$

where $\tanh(\cdot)$ is the tangent hyperbolic function. This formulation informs the system, such that the response is slow when $r_v(t)$ approaches zero, it is fast when $r_v(t)$ approaches unity, and it is moderate otherwise.

4.2. Fuzzy Self-Regulation of Adaptation Rates

The FSR system uses fuzzy logic to dynamically adjust the MRAC's inner adaptation rates in response to changes in its error dynamics [50]. It uses a set of empirically defined fuzzy logical rules and pre-calibrated membership functions (MFs) to infer accurate decisions based on the input data. Keeping in view the requirements of the buck energy conversion system, the following meta-rules are considered to devise the rule base for the FSR of the adaptation rates [48]:

1. When the system response is fast, but the error magnitude is small, large adaptation rates are selected that efficiently change the controller gains to quickly counteract the disturbance by reducing the transit speed and rejecting the overshoots.
2. When the error magnitude is large and the system response is also fast, moderate adaptation rates are selected to avoid highly disruptive (and aggressive) control application, which prevents unnecessary increment in the overshoot of the response that has already drifted significantly away from the reference.
3. When the system response is slow, irrespective of the error magnitude, the adaptation rates are reduced to decelerate the responsiveness of the controller gains. This helps apply a gentle control effort for eliminating any residual steady-state fluctuations while maintaining an accurate and smooth tracking of the reference signal.

The aforementioned rules are computationally implemented by employing a two-input FSR system that derives its input data from the error dynamics of $v_0(t)$. The normalized absolute error $e_v(t)$ and the normalized relative rate $r_v(t)$ act as the inputs of the FSR system. The normalized absolute error is computed as shown below.

$$e_v(t) = \tanh(|e(t)|^2) \tag{44}$$

Squaring the error term aids in amplifying the value of $e_v(t)$ under large error conditions and attenuating its impact under small error conditions. The fuzzification module converts the crisp input data into fuzzy linguistic variables. The input $e_v(t)$ is fuzzified into four linguistic variables defined as S—Small, SM—Small Medium, M—Medium, and

Large–Large. The input $r_v(t)$ is fuzzified into three linguistic variables defined as SL–Slow, M–Medium, MF–Medium Fast, and F–Fast. The variations in $e_v(t)$ and $r_v(t)$ are naturally normalized between 0 and 1. The output of the FSR system is denoted as $\lambda(e_v, r_v)$. It is fuzzified into four linguistic variables defined as S–Small, SM–Small Medium, M–Medium, and L–Large. The variations in $\lambda(e_v, r_v)$ are bounded between 0 and 1. The rule base constructed to realize the FSR system is shown in Table 4 [48]. A total of 16 fuzzy rules are used to carry out the fuzzy implication. To execute the fuzzy implication, the following max–min inference method is adopted.

$$\mu_i = \min(g_i(e_v), g_i(r_v)) \tag{45}$$

where μ is the degree of the MF, i is the number of rule, and $g_i(\cdot)$ is the triangular input MF of the following form.

$$g_i(f) = \begin{cases} 1 + \frac{f - c_i}{b_i^-}, & -b_i^- \leq f - c_i \leq 0 \\ 1 - \frac{f - c_i}{b_i^+}, & 0 \leq f - c_i \leq b_i^+ \\ 0, & \text{otherwise} \end{cases} \tag{46}$$

where f is the generalized representation of the input variable e_v or r_v , and b_i^- , b_i^+ , and c_i are the left half width, right half width, and centroid of the input MF, respectively. In this work, symmetrical MFs are employed to perform the fuzzy implication and aggregation. The input and output fuzzy MF waveforms are shown in Figures 7 and 8, respectively. The crisp output, $\lambda(e_v, r_v)$, is computed by using the centroid method of defuzzification as shown in (47), [50].

$$\lambda(e_v, r_v) = \frac{\sum_{i=1}^N \mu_i w_i}{\sum_{i=1}^N \mu_i} \tag{47}$$

where w is the centroid of output MF, and $N = 16$ is the total number of rules. The crisp output is fed to the following functions to deliver the time-varying adaptation rates.

$$\alpha_I(t) = \alpha_{I,o} (\varphi_{I,l} + \varphi_{I,h} \lambda(e_v, r_v)) \tag{48}$$

$$\alpha_P(t) = \alpha_{P,o} (\varphi_{P,l} + \varphi_{P,h} \lambda(e_v, r_v)) \tag{49}$$

$$\alpha_D(t) = \alpha_{D,o} (\varphi_{D,l} + \varphi_{D,h} \lambda(e_v, r_v)) \tag{50}$$

The parameters $\varphi_{z,l}$ and $\varphi_{z,h}$ (where $z = P, I, \text{ or } D$) are predetermined ratios that help decide the lower and upper limit of each adaptation rate, respectively. The selection ranges of $\varphi_{z,l}$ and $\varphi_{z,h}$ are $[0, 0.5]$ and $[0, 5]$, respectively.

Table 4. Fuzzy rule base for the FSR system [48].

$e_v \downarrow / r_v \rightarrow$	SL	M	MF	F
S	M	M	L	L
SM	SM	M	M	L
M	S	SM	M	M
L	S	S	SM	M

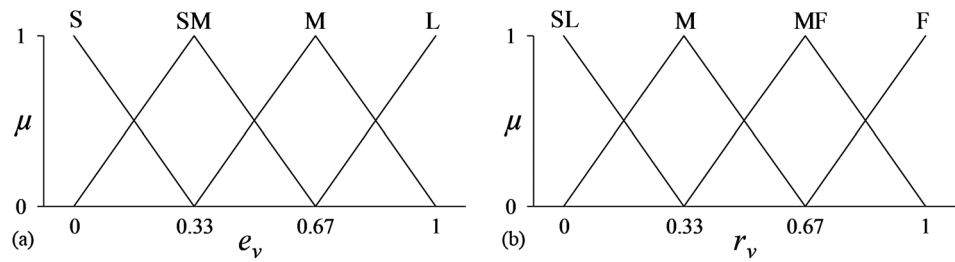


Figure 7. (a) Input fuzzy MF representing e_v , (b) Input fuzzy MF representing r_v .

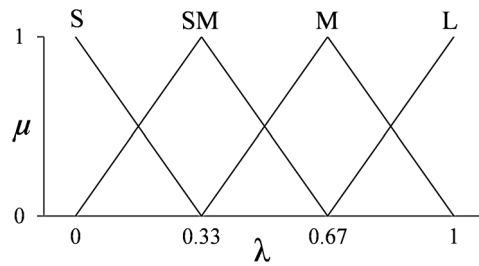


Figure 8. Output fuzzy MF representing λ .

These parameters are calibrated offline by using the tuning method discussed in Section 2.3. The selected values are $\varphi_{I,l} = 0.11$, $\varphi_{I,h} = 2.15$, $\varphi_{P,l} = 0.14$, $\varphi_{P,h} = 1.92$, $\varphi_{D,l} = 0.08$, and $\varphi_{D,h} = 1.71$. The self-adjusting matrix $\alpha(t)$ is expressed as follows:

$$\alpha(t) = \text{diag}(\alpha_I(t) \quad \alpha_P(t) \quad \alpha_D(t)) \tag{51}$$

4.3. FA-MRAC Law Formulation

The Lyapunov gain adjustment law uses the time-varying adaptation rate matrix $\alpha(t)$ to enhance the adaptability of the control law. The modified Lyapunov gain adjustment law is constituted as shown in (52).

$$\tilde{\mathbf{K}}(t) = \tilde{\mathbf{K}}(0) + \int_0^t (\alpha(t) x(t) \mathbf{B}^T \bar{\mathbf{P}} \varepsilon(t))^T dt \tag{52}$$

where $\tilde{\mathbf{K}}(t) = [\tilde{K}_I(t) \quad \tilde{K}_P(t) \quad \tilde{K}_D(t)]$ represents the time-varying state feedback gain. The state feedback gain vector $\mathbf{K} = [-3.17 \quad -1.82 \quad -0.24]$, prescribed in Section 2.3, serves as $\tilde{\mathbf{K}}(0)$ in (28). The proposed FA-MRAC law is presented below.

$$u(t) = -\tilde{\mathbf{K}}(t)x(t) \tag{53}$$

The expansion of the control law yields the following adaptive PID control equation.

$$u(t) = -\tilde{K}_P(t)e(t) - \tilde{K}_I(t) \int e(t) dt - \tilde{K}_D(t)\dot{e}(t) \tag{54}$$

The MRA-PID control law equipped with the FSR system is denoted as the FA-MRA-PID controller. The block diagram of FA-MRA-PID control law is shown in Figure 9.

From a computational point of view, the FA-MRA-PID controller does not require large training data sets for its constitution. It does not rely upon complex algorithms to compute closed-form solutions. Instead, the parameters can be updated online in a single step after every sampling interval, which allows for optimal computational resource allocation. Unlike iterative learning algorithms, the scheme does not put excessive recursive computational burden on the embedded processor. With the availability of various toolboxes and software, the implementation of the proposed control procedure is computationally viable. Each rule base comprises only 16 rules, thus, the scheme is not memory-

intensive. The digital computer’s processing power (discussed in Section 5.1) can sufficiently handle the fuzzification and defuzzification process. The scheme has no potential latency issues, since it is a two-dimensional rule base with only 16 rules.

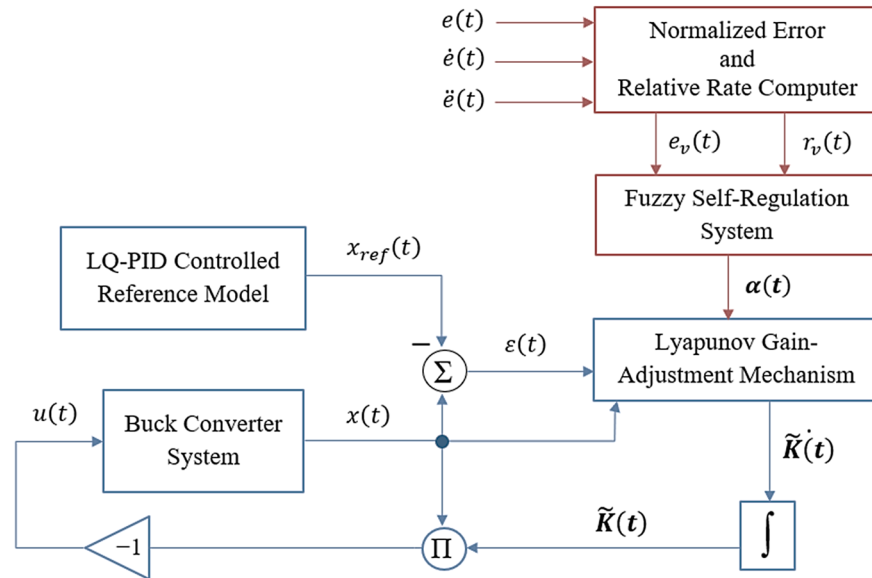


Figure 9. Block diagram of the proposed FA-MRA-PID control law.

5. Experimental Evaluation and Discussions

This section presents the results of the hardware experiments carried out to examine the efficacy of the proposed controllers under disturbances in the physical environment.

5.1. Experimental Setup

A commercial 250-watt DC–DC converter module is used to test the designed control technique experimentally. Using a variable dual output lab bench DC power supply, two +12.0 V sources are connected in series to provide a supply input of +24.0 V to the converter module. Figure 10 presents the complete hardware schematic [41]. Dedicated voltage divider circuits are used to measure the real-time fluctuations in v_o and v_{in} . An 8-bit embedded microcontroller is used to obtain the raw analog sensor readings at a 0.5 kHz sampling frequency. The digitized sensor data are serially transmitted to a MATLAB-based computer application for control computations at a baud rate of 9600 bps. The MATLAB/Simulink R2018b software is used to implement the control application and to carry out the simulations. For this purpose, a 32-bit and 900 MHz computer with 1.0 GB RAM is adopted. The real-time voltage fluctuations are also graphically represented by using MATLAB software. After every sampling instant, the computed control signal is serially transmitted to the microcontroller, which converts it into an equivalent pulse-width-modulated (PWM) signal and applies it to drive the transistor Q_1 . A logically inverted command of this PWM signal is applied to transistor Q_2 . The transistors are driven at a switching frequency of 100 kHz. The disturbance rejection capacity of the prescribed controllers is examined via customized experiments that are designed to emulate practical disturbance scenarios for the buck converter system. To administer a +12.0 V step fluctuation in the system’s v_{in} , the supply voltage can be adjusted by flipping the switch “S” between positions A and B, as seen in Figure 6. Typically, the switch Q_3 is inactive, which allows only a single load resistor to stay coupled with the circuit. To introduce a 50% step decrement in the system’s load R_L , the switch Q_3 is turned, which brings the two identical resistances in parallel to each other. This arrangement reduces the overall load resistance to $0.5R_L$. Figure 11 depicts the hardware setup used for the experimentation [41].

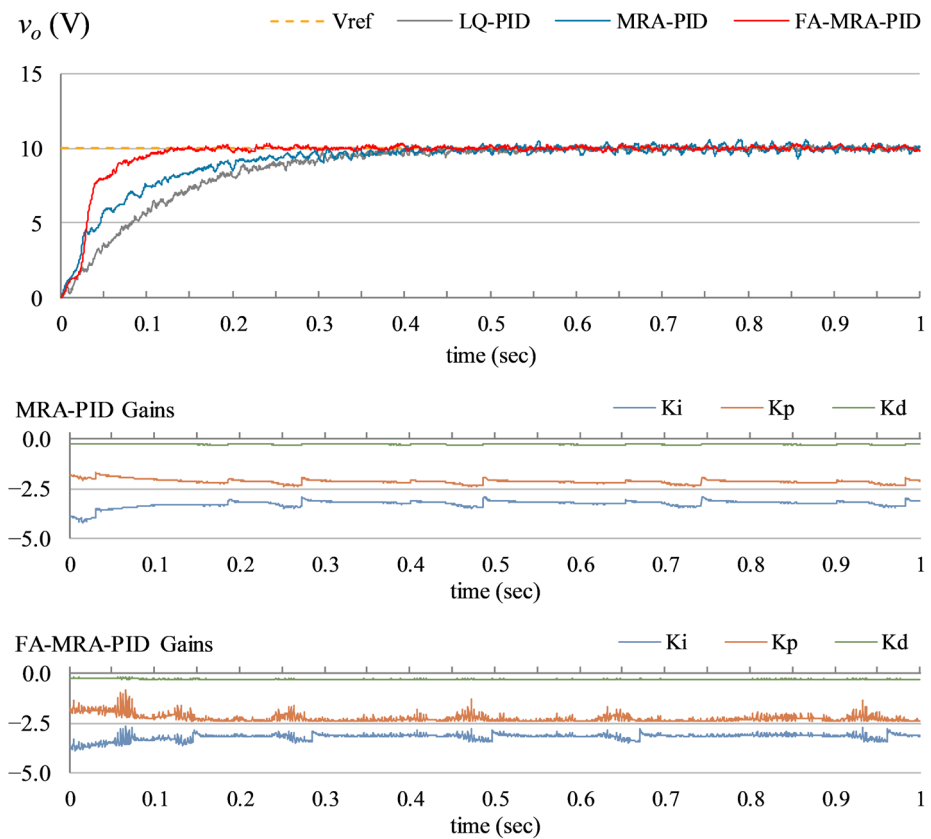


Figure 12. Response of the system under nominal conditions.

- B. *Load disturbance rejection:* This test case is used to examine the controller’s ability to reject step disturbances in the converter’s load. The said experiment is conducted by activating the switch Q_3 at $t = 0.6$ s, which administers a 50% step decrement in the system’s load resistance. The corresponding fluctuations recorded in $v_o(t)$ are shown in Figure 13.
- C. *Input disturbance compensation:* This test case is used to examine the controller’s adaptability to compensate for step disturbances in the converter’s v_{in} . The said experiment is conducted by flipping the switch S at $t = 0.6$ s from the position A to position B, as shown in Figure 5, which decreases the converter’s v_{in} from +24.0 V to +12.0 V. The consequent perturbations in the system’s $v_o(t)$ are shown in Figure 14.

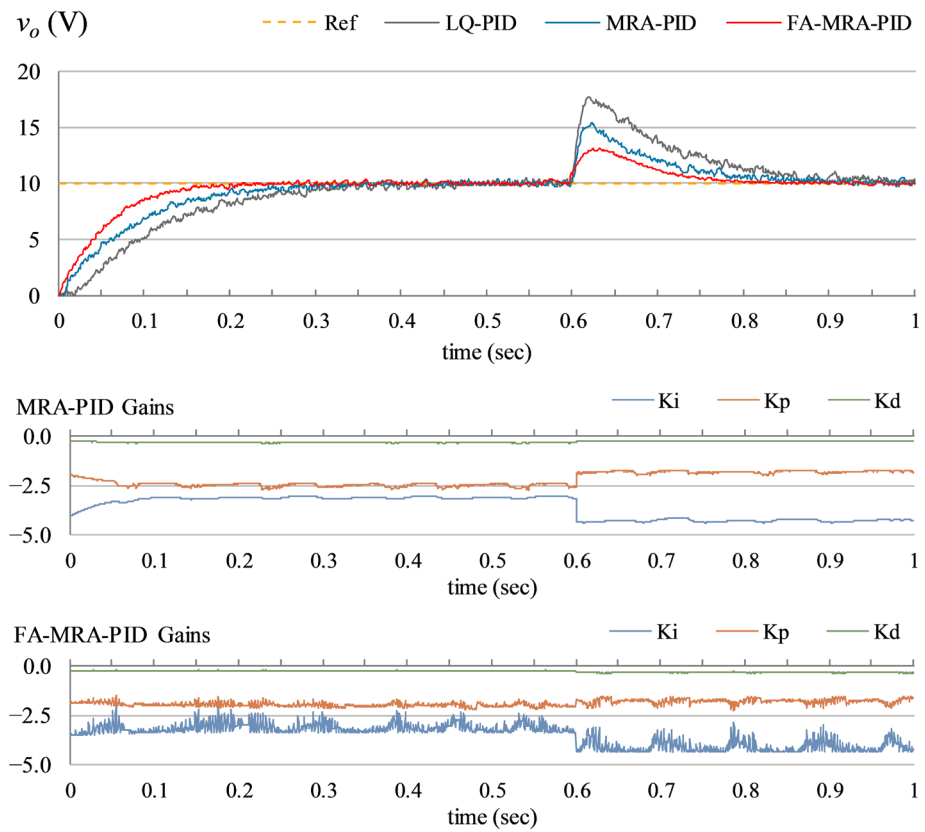


Figure 13. Response of the system under load step disturbances.

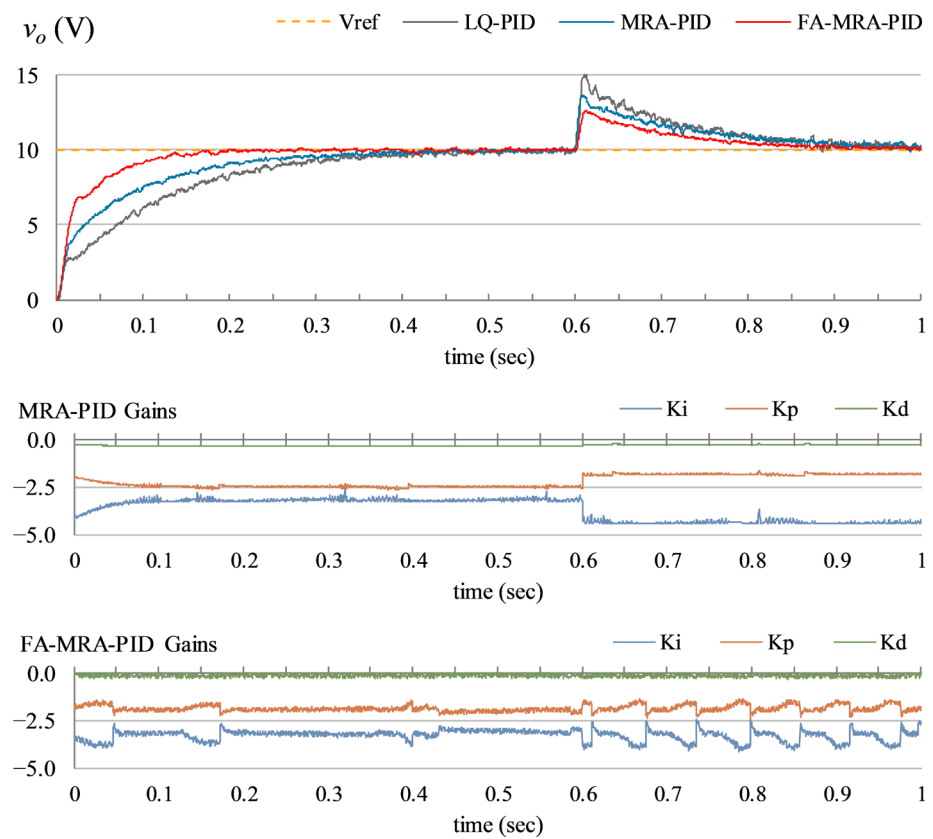


Figure 14. Response of the system under input step fluctuations.

5.3. Discussion

The results of the aforementioned experiments are examined in terms of the following key performance metrics (KPMs).

- e_{rms} : The root mean squared value of error in v_o , $\Sigma \sqrt{\frac{(e(n))^2}{n}}$.
- t_{rise} : The time taken by v_o to commute from 10% to 90% of the v_{ref} .
- t_{set} : The time taken by v_o to settle within $\pm 2\%$ of v_{ref} after the initial startup.
- OS: The peak overshoot in v_o contributed by the initial startup.
- M_p : The peak overshoot in v_o contributed by the load or input disturbance.
- t_{rec} : The time taken by v_o to recover and settle within $\pm 2\%$ of v_{ref} after disturbance.

These KPMs are typically used to accurately assess the buck converter system's time domain behavior [41]. Table 5 presents the quantitative analysis of the experimental outcomes of the FA-MRA-PID controller (formulated in Section 4) benchmarked against the traditional MRA-PID controller (formulated in Section 3) and the LQ-PID controller (formulated in Section 2). The enhanced resilience of the FA-MRA-PID control law in each experiment is benchmarked and validated by the experimental results.

In **Experiment A** (Figure 12), the LQ-PID control manifests the slowest transient recovery behavior followed by prolonged steady-state fluctuations. The time domain performance is improved by the MRA-PID controller, which shows comparatively faster transient recovery speed followed by smaller overshoots and steady-state fluctuations. The proposed FA-MRA-PID controller offers the most time-efficient response. It transits quickly to the reference signal while robustly damping the overshoot and ensuing oscillations. The rapid yet consistent fluctuations in the time-varying controller gains, evident during the initial start-up phase of the response, validate the proposed controller's enhanced responsiveness to the changes in the system's operating conditions. The gains variations are large and disruptive at the beginning of the transient state. These variations gradually decay when the response approaches the steady state. Under nominal conditions, the proposed controller reduces the system's e_{rms} by 22.9%, t_{rise} by 33.3%, t_{set} by 47.5%, and OS by 3.4% as compared to the baseline LQ-PID controller. The proposed controller improves the system's e_{rms} by 16.7%, t_{rise} by 28.6%, t_{set} by 30.1%, and OS by 39.1% as compared to the traditional MRA-PID controller.

In **Experiment B** (Figure 13), the modeling uncertainties caused by the load step disturbance severely impair the performance of the fixed gain LQ-PID controller, which results in the system exhibiting the slowest transient response speed and significant overshoots and undershoots.

Table 5. Summary of experimental results.

Experiment	KPM		Control Law		
	Symbol	Unit	LQ-PID	MRA-PID	FA-MRA-PID
A	e_{rms}	V	0.055	0.042	0.035
	t_{rise}	sec.	0.21	0.14	0.10
	OS	V	0.29	0.46	0.28
	t_{set}	sec.	0.40	0.30	0.21
B	e_{rms}	V	0.085	0.062	0.046
	M_p	V	7.74	5.40	3.09
	t_{rec}	sec.	0.26	0.21	0.16
C	e_{rms}	V	0.054	0.042	0.029
	M_p	V	5.07	3.65	2.63
	t_{rec}	sec.	0.35	0.31	0.27

It minimizes the peak magnitude of the overshoots and undershoots brought on by load disturbance. The controller gains demonstrate a rapid rate of change during the perturbed state, and vice versa, which significantly increases the adaptability of the control law under bounded exogenous disturbances. Under load disturbance conditions, the proposed controller reduces the system's e_{rms} by 43.5%, M_p by 60.1%, and t_{rec} by 38.5% as compared to the baseline LQ-PID controller. Moreover, the proposed controller reduces the system's e_{rms} by 25.8%, M_p by 42.8%, and t_{rec} by 23.8% as compared to the traditional MRA-PID controller.

In **Experiment C** (Figure 14), the introduction of input step disturbance causes abrupt state fluctuations, to which the FSR system of the proposed controller reacts swiftly and efficiently adapts the controller gains. The variation rate of the controller gains becomes highly disruptive under the disturbance condition, which helps the control law to quickly react by flexibly tightening the damping control effort, and vice versa. This arrangement results in a reasonably robust disturbance rejection behavior, which delivers relatively faster transit times and minimal post-disturbance oscillations. The LQ-PID and MRA-PID controllers exhibit poor and mediocre performances in this experiment as well, respectively. The suggested FA-MRA-PID controller precisely tracks the reference voltage while successfully damping oscillations brought on by the external disturbance. Under load disturbance conditions, the proposed controller reduces the system's e_{rms} by 46.3%, M_p by 48.1%, and t_{rec} by 22.8% as compared to the LQ-PID controller. Moreover, the proposed controller reduces the system's e_{rms} by 30.9%, M_p by 27.9%, and t_{rec} by 12.9% as compared to the traditional MRA-PID controller.

The suggested FA-MRA-PID controller precisely tracks the reference voltage while successfully damping oscillations brought on by the external disturbance. The enhanced robustness and response speed are credited to the relate-rate-derived FSR system used with the MRA-PID controller. The FSR system increases the system's self-learning ability and enables it to execute effective autonomous self-tuning of the controller gains as the error conditions vary. The improved responsiveness of the proposed controller is evident from the abrupt and persistent fluctuations displayed by the gains of the FA-MRA-PID controller in Figures 12–14.

The proposed FA-MRA-PID control procedure is highly scalable. It can be easily modified and applied to control the output voltage of any class of DC–DC power electronic converter, since it only requires the nominal state space model of the conversion system to formulate the LQ-PID-regulated reference model, along with a customized set of adaptation rate adjustment functions, as the a priori information. With the aforementioned requirements fulfilled, apart from the DC–DC converters, the proposed control scheme can be extended and applied to control under-actuated robotic and mechatronic systems.

5.4. Comparison with a State-of-the-Art Control Law

To confirm the effectiveness of the proposed FA-MRA-PID controller in comparison to the modern controllers, its performance is compared with a fractional-order LQ-optimized PID voltage controller tasked with robust compensation of disturbances in DC–DC buck converters [41]. The fractional order PID control law is presented as shown below.

$$u(t) = K_i(G^{-\alpha}e(t)) + K_p e(t) + K_d(G^{\beta}e(t)) \quad (55)$$

where $K_i = -3.162$, $K_p = -1.977$, and $K_d = -0.315$ are the integral, proportional, and derivative gains of the PID control law, respectively. The terms $G^{-\alpha}$ and G^{β} represent the fractional order integral and differential operators, respectively. The terms $\alpha = 0.92$ and $\beta = 0.74$ are the pre-calibrated fractional orders of the said operators [41]. The said fractional-order PID (denoted as $PI^{\alpha}D^{\beta}$) controller is selected for comparative analysis with the proposed FA-MRA-PID controller because its real-time behavior is examined using the same experimental setup and test cases as this study. Table 6 quantifies the comparative performance analysis along with the percentage improvement recorded for every

performance metric being analyzed. The KPM $e_{rms,ss}$ in Table 6 represents the root mean squared value of error recorded for the steady-state portion of the response only. The quantitative study validates that in nearly all testing scenarios, the FA-MRA-PID controller exhibits a relatively better reference tracking accuracy and disturbance rejection capability than the $PI^{\alpha}D^{\beta}$ controller.

Table 6. Comparison with $PI^{\alpha}D^{\beta}$ controller.

Experiment	KPM		Control Law		Percentage Improvement
	Symbol	Unit	$PI^{\alpha}D^{\beta}$ [41]	FA-MRA-PID (proposed)	
A	$e_{rms,ss}$	mV	6.56	6.15	6.3 %
	t_{rise}	msec.	0.15	0.10	33.3 %
	OS	V	n/a	0.28	n/a
	t_{set}	sec.	0.23	0.21	8.7 %
B	M_p	V	3.48	3.09	11.2 %
	t_{rec}	sec.	0.18	0.16	11.1 %
C	M_p	V	4.66	2.63	43.5 %
	t_{rec}	sec.	0.35	0.27	22.9 %

n/a, not available.

6. Conclusions

This article methodically designs and implements a novel self-regulating MRA-PID control law that aims to improve the robustness of DC–DC energy conversion systems against modeling uncertainties and disturbances. To concurrently improve the system's response speed as well as error rejection, a pre-calibrated two-input FSR is augmented with the MRA-PID control law that self-regulates the adaptation rates as the system transits from transient to steady-state, and vice versa. The FSR is formulated as a nonlinear function of the error and relative rate of the system's output voltage response. The inclusion of relative rate feedback is very beneficial in this application as it optimizes the system's self-learning, and thus, self-reasoning capability. Consequently, it helps the system execute effective parameter adjustment decisions as per the changes in the dynamic speed of the response when it drifts away from the reference, or converse.

The proposed augmentation considerably increases the degrees of freedom of the MRAC law. The time domain profiles and gain variations exhibited by the proposed controller, under different experimental conditions, clearly validate its enhanced adaptability, temporal efficiency, superior reference tracking accuracy, and stronger robustness against the model variations caused by the input and load step fluctuations. In the future, the proposed control scheme can be extended and applied to other types of DC–DC converter systems. Furthermore, neural and neuro-fuzzy adaptation mechanisms can be used, instead of the proposed FSR, to self-regulate the inner adaptation rates of MRACs and investigate their implications on the system's response speed and sensitivity to disturbances.

Author Contributions: Conceptualization, O.S.; methodology, O.S.; software, O.S. and K.R.A.; validation, J.I.; formal analysis, O.S.; investigation, O.S. and K.R.A.; resources, J.I.; data curation, K.R.A.; writing—original draft preparation, O.S.; writing—review and editing, J.I.; visualization, J.I.; supervision, J.I.; project administration, J.I. All authors have read and agreed to the published version of the manuscript.

Funding: This research received no external funding.

Data Availability Statement: The authors declare that the data analyzed during this study to support the findings will be made available on reasonable request.

Conflicts of Interest: The authors declare no conflict of interest.

References

1. Alfred, D.; Czarkowski, D.; Teng, J. Reinforcement Learning-Based Control of a Power Electronic Converter. *Mathematics* **2024**, *12*, 671.
2. Shenoy, P.S.; Amaro, M.; Morroni, J.; Freeman, D. Comparison of a Buck Converter and a Series Capacitor Buck Converter for High-Frequency, High-Conversion-Ratio Voltage Regulators. *IEEE Trans. Pow. Electron.* **2016**, *31*, 7006–7015.
3. Abdurraqeab, A.M.; Al-Shamma'a, A.A.; Alkuhayli, A.; Noman, A.M.; Addoweesh, K.E. RST Digital Robust Control for DC/DC Buck Converter Feeding Constant Power Load. *Mathematics* **2022**, *10*, 1782.
4. Rumbo-Morales, J.Y.; Gómez-Radilla, J.; Ortiz-Torres, G.; Sorcia-Vázquez, F.D.J.; Buenabad-Arias, H.M.; López-Osorio, M.A.; Torres-Cantero, C.A.; Ramos-Martinez, M.; Juárez, M.A.; Calixto-Rodríguez, M.; et al. Geometric Control and Structure-at-Infinity Control for Disturbance Rejection and Fault Compensation Regarding Buck Converter-Based LED Driver. *Mathematics* **2024**, *12*, 1277.
5. Chen, G.; Deng, Y.; Dong, J.; Hu, Y.; Jiang, L.; He, X. Integrated Multiple-Output Synchronous Buck Converter for Electric Vehicle Power Supply. *IEEE Trans. Veh. Technol.* **2017**, *66*, 5752–5761.
6. Bereš, M.; Kováč, D.; Vince, T.; Kováčová, I.; Molnár, J.; Tomčíková, I.; Dziak, J.; Jacko, P.; Fecko, B.; Gans, Š. Efficiency Enhancement of Non-Isolated DC-DC Interleaved Buck Converter for Renewable Energy Sources. *Energies* **2021**, *14*, 4127.
7. Sreekumar, C.; Agarwal, V. Hybrid control approach for the output voltage regulation in buck type DC-DC converter. *IET Electr. Power Appl.* **2007**, *1*, 897–906.
8. Saoudi, M.; El-Sayed, A.; Metwally, H. Design and implementation of closed-loop control system for buck converter using different techniques. *IEEE Aerosp. Electron. Syst. Mag.* **2017**, *32*, 30–39.
9. Wang, S.; Li, S.; Su, J.; Li, J.; Zhang, L. Extended state observer-based nonsingular terminal sliding mode controller for a DC-DC buck converter with disturbances: Theoretical analysis and experimental verification. *Int. J. Control* **2023**, *96*, 1661–1671.
10. Olalla, C.; Queinnec, I.; Leyva, R.; El-Aroudi, A. Robust optimal control of bilinear DC-DC converters. *Control Eng. Pract.* **2011**, *19*, 688–699.
11. Mariethoz, S.; Almer, S.; Baj, M.; Beccuti, A.G.; Patino, D.; Wernrud, A.; Buisson, J.; Cormerais, H.; Geyer, T.; Fujioka, H.; et al. Comparison of hybrid control techniques for buck and boost DC-DC converters. *IEEE Trans. Control Syst. Technol.* **2010**, *18*, 1126–1145.
12. Rajamani, M.P.E.; Rajesh, R.; Willjuice Iruthayarajan, M. Design and experimental validation of PID controller for buck converter: A multi-objective evolutionary algorithms based approach. *IETE J. Res.* **2023**, *69*, 21–32.
13. Kapat, S.; Krein, P.T. Formulation of PID control for DC-DC converters based on capacitor current: A geometric context. *IEEE Trans. Pow. Electron.* **2011**, *27*, 1424–1432.
14. Chincholkar, S.; Tariq, M.; Poshtan, M.; Sharaf, M. Normalized Error-Based PI Controller and Its Application to the DC-DC Buck Converter. *Mathematics* **2024**, *12*, 240.
15. Ghamari, S.M.; Narm, H.G.; Mollae, H. Fractional-order fuzzy PID controller design on buck converter with antlion optimization algorithm. *IET Control Theory Appl.* **2022**, *16*, 340–352.
16. Warriar, P.; Shah, P. Design of an Optimal Fractional complex order PID controller for buck converter. *J. Rob. Control* **2023**, *4*, 243–262.
17. Naik, B.B.; Mehta, A.J. Sliding mode controller with modified sliding function for DC-DC Buck Converter. *ISA Trans.* **2017**, *70*, 279–287.
18. Ding, S.; Zheng, W.X.; Sun, J.; Wang, J. Second-order sliding-mode controller design and its implementation for buck converters. *IEEE Trans. Ind. Inform.* **2017**, *14*, 1990–2000.
19. Huangfu, Y.; Zhuo, S.; Rathore, A.K.; Breaz, E.; Nahid-Mobarekeh, B.; Gao, F. Super-twisting differentiator-based high order sliding mode voltage control design for DC-DC buck converters. *Energies* **2016**, *9*, 494.
20. Kaplan, O.; Bodur, F. Second-order sliding mode controller design of buck converter with constant power load. *Int. J. Control* **2023**, *96*, 1210–1226.
21. Dong, W.; Li, S.; Fu, X.; Li, Z.; Fairbank, M.; Gao, Y. Control of a buck DC/DC converter using approximate dynamic programming and artificial neural networks. *IEEE Trans. Circuits Syst. I Reg. Papers* **2021**, *68*, 1760–1768.
22. Sorouri, H.; Sedighzadeh, M.; Oshnoei, A.; Khezri, R. An intelligent adaptive control of DC-DC power buck converters. *Int. J. Elect. Pow. Energy Syst.* **2022**, *141*, 108099.
23. Nizami, T.K.; Mahanta, C. An intelligent adaptive control of DC-DC buck converters. *J. Franklin Inst.* **2016**, *353*, 2588–2613.
24. Saleem, O.; Shami, U.T.; Mahmood-ul-Hasan, K. Time-optimal control of DC-DC buck converter using single-input fuzzy augmented fractional-order PI controller. *Int. Trans. Electr. Energy Syst.* **2019**, *29*, e12064.
25. Behih, K.; Benmahammed, K.; Bouchama, Z.; Harmas, M.N. Real-time investigation of an adaptive fuzzy synergetic controller for a DC-DC buck converter. *Eng. Technol. Appl. Sci. Res.* **2019**, *9*, 4984–4989.
26. Saleem, O.; Rizwan, M. Performance optimization of LQR-based PID controller for DC-DC buck converter via iterative-learning-tuning of state-weighting matrix. *Int. J. Numer. Mod.* **2019**, *32*, e2572.
27. Junior, L.A.M.; Valle, R.L.; Ferreira, A.A.; Barbosa, P.G.; Montagner, V.F. A LQR design with rejection of disturbances and robustness to load variations applied to a buck converter. *Eletrônica Potência* **2016**, *21*, 7–15.
28. Danayiyen, Y.; Altas, I.; Sahin, E. Model Predictive Control of a DC-DC Buck Converter. *Sigma J. Eng. & Nat. Sci.* **2017**, *8*, 91–97.
29. Chen, Y.; Lu, Y.; Luo, W. Model predictive control of double-input buck converters. *J. Pow. Electron.* **2021**, *21*, 941–950.

30. Rigatos, G.; Siano, P.; Sayed-Mouchaweh, M. Adaptive neurofuzzy H-infinity control of DC–DC voltage converters. *Neural Comput. Appl.* **2020**, *32*, 2507–2520.
31. Boukerdja, M.; Chouder, A.; Hassaine, L.; Bouamama, B.O.; Issa, W.; Louassaa, K. H^∞ based control of a DC/DC buck converter feeding a constant power load in uncertain DC microgrid system. *ISA Trans.* **2020**, *105*, 278–295.
32. Ghamari, S.M.; Khavari, F.; Mollaee, H. Adaptive backstepping controller design for DC/DC buck converter optimised by grey wolf algorithm. *IET Energy Syst. Integr.* **2024**, *6*, 18–30.
33. Saadat, S.A.; Ghamari, S.M.; Mollaee, H. Adaptive backstepping controller design on Buck converter with a novel improved identification method. *IET Control Theory Appl.* **2022**, *16*, 485–495.
34. He, W.; Namazi, M.M.; Guerrero, J.M. Adaptive Energy-Based Control for Buck Converter with a Class of Nonlinear Loads. *IEEE Trans. Circuit Syst. II* **2022**, *69*, 4869–4873.
35. Chouya, A.; Boureguig, K. Adaptive Control with MRAC Regulator for DC-DC Buck Converter. *Int. J. Control Syst. Robot.* **2022**, *7*, 13–26.
36. Islam, M.; Abdul Ghaffar, A.F.; Sulaeman, E.; Ahsan, M.M.; Kouzani, A.Z.; Mahmud, M.P. Performance analysis of PI and DMRAC algorithm in buck–boost converter for voltage tracking in electric vehicle using simulation. *Electronics* **2021**, *10*, 2516.
37. Qureshi, M.A.; Musumeci, S.; Torelli, F.; Reatti, A.; Mazza, A.; Chicco, G. A novel model reference adaptive control approach investigation for power electronic converter applications. *Int. J. Electr. Pow. Energy Syst.* **2024**, *156*, 109722.
38. Saleem, O.; Rizwan, M.; Mahmood-ul-Hasan, K.; Ahmad, M. Performance enhancement of multivariable model reference optimal adaptive motor speed controller using error-dependent hyperbolic gain functions. *Automatika* **2020**, *61*, 117–131.
39. Dinakin, D.; Oluseyi, P. Fuzzy-Optimized model reference adaptive control of interacting and noninteracting processes based on MIT and Lyapunov rules. *Turkish J. Eng.* **2021**, *5*, 141–153.
40. Saleem, O.; Rizwan, M.; Awan, F.G. Robustification of the state-space MRAC law for under-actuated systems via fuzzy-immunological computations. *Sci. Prog.* **2022**, *105*, 1–26.
41. Saleem, O.; Awan, F.G.; Mahmood-ul-Hasan, K.; Ahmad, M. Self-adaptive fractional-order LQ-PID voltage controller for robust disturbance compensation in DC-DC buck converters. *Int. J. Numer. Model.* **2020**, *33*, e2718.
42. Tan, G.Q.; Chen, Y.H.; Gu, L. LQR based optimal PID control for buck converter. *Appl. Mech. Mater.* **2014**, *687*, 3221–3226.
43. Lewis, F.L.; Vrabie, D.; Syrmos, V.L. *Optimal control*; John Wiley & Sons: New Jersey, USA, **2012**.
44. Saleem, O.; Iqbal, J. Complex-order PID controller design for enhanced blood-glucose regulation in Type-I diabetes patients. *Meas. Control* **2023**, *56*, 1811–1825.
45. Tian, T.; Hou, X.; Yan, F. A Novel MRAC Scheme for Output Tracking. *Mathematics* **2022**, *10*, 2384.
46. Chen, K.Y. Model reference adaptive minimum-energy control for a mechatronic elevator system. *Optim. Control Appl. Method.* **2017**, *38*, 3–18.
47. Astrom, K.J.; Wittenmark, B. *Adaptive Control*, 3rd ed; Pearson Education: London, UK, 1995.
48. Chen, K.Y.; Tung, P.C.; Tsai, M.T.; Fan, Y.H. A self-tuning fuzzy PID-type controller design for unbalance compensation in an active magnetic bearing. *Expert. Syst. Appl.* **2009**, *36*, 8560–8570.
49. Saleem, O. An enhanced adaptive-LQR procedure for under-actuated systems using relative-rate feedback to dynamically re-configure the state-weighting-factors. *J. Vib. Control* **2023**, *29*, 2316–2331.
50. Nguyen, H.T.; Prasad, N.R.; Walker, C.L.; Walker, E.A. *A First Course in Fuzzy and Neural Control*, 1st ed; Chapman and Hall/CRC: London, UK, 2002.

Disclaimer/Publisher’s Note: The statements, opinions and data contained in all publications are solely those of the individual author(s) and contributor(s) and not of MDPI and/or the editor(s). MDPI and/or the editor(s) disclaim responsibility for any injury to people or property resulting from any ideas, methods, instructions or products referred to in the content.